De Certaines et al. EPJ Nonlinear Biomedical Physics (2015) 3:3
DOI 10.1140/s40366-015-0017-1

EPJ Nonlinear Biomedical Physics
a SpringerOpen Journal

EPJ.org

REVIEW Open Access

Application of texture analysis to muscle MRI: 1-What kind of information should be expected from texture analysis?

Jacques D De Certaines[1,2*], Thibaut Larcher[3], Dorota Duda[4], Noura Azzabou[1,2], Pierre-Antoine Eliat[5], Luis M Escudero[6], Antonio MG Pinheiro[7], Guanyu Yang[8], Jean-Louis Coatrieux[9], Eduard Snezkho[10], Alexey Shukelovich[1], Manuela Pereira[7] and Richard A Lerski[11]

* Correspondence: jacques.de-certaines@orange.fr
[1]Institute of Myology, NMR laboratory, Paris, France
[2]CEA, I2BM, MIRCen, NMR laboratory, Paris, France
Full list of author information is available at the end of the article

Abstract

Several previous clinical or preclinical studies using computerized texture analysis of MR Images have demonstrated much more clinical discrimination than visual image analysis by the radiologist. In muscular dystrophy, a discriminating power has been already demonstrated with various methods of texture analysis of magnetic resonance images (MRI-TA). Unfortunately, a scale gap exists between the spatial resolutions of histological and MR images making a direct correlation impossible. Furthermore, the effect of the various histological modifications on the grey level of each pixel is complex and cannot be easily analyzed. Consequently, clinicians will not accept the use of MRI-TA in routine practice if TA remains a "black box" without clinical correspondence at a tissue level. A goal therefore of the multicenter European COST action MYO-MRI is to optimize MRI-TA methods in muscular dystrophy and to elucidate the histological meaning of MRI textures.

Review

Several methods of image post-processing have been developed for Texture Analysis of Magnetic Resonance images (MRI-TA) and have already demonstrated stimulating results in a large range of pre-clinical or clinical applications [1]; MRI-TA usually provides much more clinical discrimination than visual analysis of MR images by the radiologist [2]; visual analysis (about 100 grey level can be discriminated) is ten times less sensitive to fine and local grey level changes than computer analysis (about 1000 grey level by using computer detection). There is presently no well-established consensus concerning the limits of texture visual perception but it is clear that texture represented by higher orders statistics can only be discriminated by computerized image analysis.

In normal versus dystrophic muscles, a discriminating power at an early stage and during disease evolution has been demonstrated with various MRI-TA methods: some MRI texture parameters in healthy or diseased skeletal muscle have previously been related to fat infiltration [3,4] to the loss of orientation of muscle fibers [3], to the disturbance of perimysium [3], to the mean size of necrotic and regeneration foci [5], to the proportion of oxidative myofibers [5], to the endomysal fibrosis [5] and collagen content [4] or to the heterogeneity of myofiber size [5].

Unfortunately, a scale gap exists between the spatial resolutions of histological and MR images making a direct correlation impossible. Furthermore, the effect of the various histological modifications on the grey level of each pixel is complex and cannot be easily analyzed. Consequently, clinicians will not accept the use of MRI-TA in routine practice if TA remains a "black box" without clinical correspondence at a tissue level. The goal of this paper is then to try and present an early analysis of MRI-TA in relation to histological changes. Golden Retriever Muscular Dystrophy (GRMD) is the only animal model with relevance to human Duchenne muscular dystrophy (DMD): it has been selected for MRI-TA tests under the auspices of the European COST action MYO-MRI aiming to optimize TA methods and to try to elucidate the histological meaning of MRI textures.

Perception of visual textures

To Rosentholtz [6] a visual texture is the consequence of the reflection of a surface that leads to variations of the light that reaches our eyes. Typically these variations are considered a visual texture when they create a visual stimulus defined by repeated patterns. They can be regular (textiles, brick walls, honeycomb), random (forest floor) or in between (wood grain) [7]. Although a human observer has the ability to recognize textures with multiple properties, it is often difficult to define them. In fact the ability to recognize textures is a very important part of the visual system recognition mechanism. Moreover, the visual system easily performs the perceptual organization (definition of different regions, objects and structures of an image) using multiple visual cues. Texture similarity plays an important role on defining this segmentation process [8,9]. The earlier work on texture perception of Julesz [10] considers that human observers could only discriminate textures which differ on the first and second-order pixels statistics. However, Julesz himself later opposed that conjecture [11] and considered that some third [12] or forth [13] order pixel statistics could also be discriminated.

Sufficiently rich statistical models can capture texture structures up to a certain level. In fact, the most recent models of texture analysis are based on multiscale filtering models rather than higher-order pixels statistics [14], suggesting that the local processes used by human observers to compare textures might be more appropriate for texture detection [15]. As an example, Heeger and Bergen [16] defined a descriptor based on first order statistics of the outputs of multiscale filters, either with or without orientation. This work was extended by Portilla and Simoncelli [17] by adding second order statistics (joint statistics) of the multi scale responses. The successor of this model demonstrates that a multidimensional set of image statistics results in the capture of texture information that might be lost on the visual representation.

These theories all try to do texture segmentation with similar mechanisms to those that exist in the early vision. However, according to Rosenholtz [6] the visual system identifies texture boundaries in an intelligent way, not in the early vision system. Hence, texture identification is the result of statistical differences. The perception of different textures can be the result of different mean texture orientations, or because of the orientation variances. The perception of two different textures with the same mean and variance becomes typically difficult for human observers. This can happen for instance if one of the textures is unimodal and the other is bimodal [18]. This limitation

results from the fact that texture segmentation involves local statistics instead of global statistics [19]. Tests using significance differences in mean orientation, mean contrast, orientation variance, and contrast variance reveal that the observers could define different regions. Rosenholtz even suggests that the human brain might have a mechanism comparable to a statistical test when defining a texture boundary. In fact the human brain might perform an earlier preprocessing of the information similar to the preprocessing of the texture image using a set of proper of multiscale filters. However, this processing step shall be complemented with sufficiently rich statistical models that provide the information for the detection of different textures and to define the image structure.

The "scale gap" between histology and MRI

Spatial resolution in MRI is limited by the NMR signal intensity depending on the number of detectable nuclear spins N(H) into the voxel, the magnetic field B_0 and the number of excitations NEX. Increasing the voxel size decreases the texture information into the image; fortunately, as muscle fibers are longitudinally oriented in skeletal muscles, 2D-MRI slice thickness can be increased without drastic loss of in-plane information when MRI is performed in the transverse plane with reference to the muscle fibers orientation. However, in 3D MRI-TA the voxel has to be isometric. The signal to noise ratio (SNR) increases with the static magnetic field with the relation $SNR = f(B_0^{3/2})$; however to increase B_0 also increases the number of artifacts such as the susceptibility artifact. SNR also depends on NEX with the relation $SNR = f(NEX^{1/2})$. Therefore the optimization of the SNR can only be a compromise between these different parameters; for instance, if we increase B_0, we increase SNR but the longitudinal relaxation time T1 is longer and then the repetition time TR has to be increased and NEX has to be decreased for the same total acquisition time. This subtle compromise between B_0 field, voxel size and NEX has presently induced an increase of the B_0 field of the marketed MRI devices up to 3T in clinical routine and 4 to 8 Tesla in research; the in-plane resolution is usually around $1mm^2$ in clinical routine and up to a few hundred μm^2 in research. For instance, previous muscle 2D MRI-TA studies have used rather similar voxel sizes: the pixel size was $0.8 \times 0.8\ mm^2$ with a slice thickness of 3 mm [20] or 6 mm [21] at 1.5T, or $0.7 \times 0.7\ mm^2$ with a slice thickness of 4 mm at 3T [22]. For the only one previous study on muscle 3D MRI-TA, the voxel size was 1mm × 1mm × 1mm [23]. Therefore in order to increase spatial resolution and contrast-to-noise ratio, MRI devices are often selected with a high magnetic field strength though field cycling experiments have demonstrated that the T1 contrast between different tissues usually decreases from 1 to 100 MHz. However, if the T1 contrast between muscle and fat mainly determines the MRI texture, then it has been demonstrated that there is a better result at high field as shown in Table 1.

There remains a large scale gap between MRI and histology, even when using a high field MRI device, because the resolution of MRI in routine practice cannot be sufficiently increased.

Table 1 Frequency dependence of T1 contrast between muscle and fat (calculated from the ex-vivo data collected by P.A.Bottomley et al. [24])

NMR frequency	20 MHz	40 MHz	60 MHZ	80 MHz	100 MHz
T1 contrast: (muscle-fat)/muscle	0.50	0.60	0.68	0.70	0.74

What MRI factors dictate the pixel grey level?

Several tissue NMR parameters determine the grey level in each voxel: the spin–lattice relaxation time T1, the spin-spin relaxation time T2, the spin density N(H) and the spin displacements (flow and diffusion). For instance, in the classical spin-echo (SE) pulse sequence, the MRI signal intensity I for solid tissues is given by:

$$I = f\left[k{v_o}^{1/3}N(H)\left(1 - e^{-TR/T1}\right)e^{-TE/T2}\right]$$

where:

k is a parameter related to the MRI device

v_o is the resonance frequency, varying from around 20 MHz (low field MRI devices) to around 90 MHz in current routine clinical usage and up to 350 MHz in pre-clinical and clinical research.

TR is the repetition time between two pulse sequences (i.e. the time for relaxing spin system).

TE is the echo time.

What are the values of T1 and T2 in human skeletal muscle and what is their frequency dependence? Mean T1 and T2 data collected from 13 MRI units clearly demonstrate a highly different field dependence between T1 and T2 measured in-vivo (Table 2). This in-vivo T1 field dependence is rather similar to the theoretical fits calculated from ex-vivo data by Fischer, Bottomley or Escanye (for review, see [25]).

Research conducted over the last forty years has shown that the T1 and T2 variations are related to the ratio between lipids and bound or free water in the tissues. Protons presenting very short relaxation times (for instance protons from proteins or from highly bound water) do not contribute to the MRI signal. Each one of these parameters is specifically more sensitive to some tissue modifications at a molecular level: for instance, fibrosis, corresponding to an increase of collagen fibers with an increase of associated bound water, decreases the T2; an oedema resulting from an increase of free water induces a T1 increase, etc. These specific effects of histological changes on T1, T2 and N(H) are not always in the same direction inducing a global result also depending on the amount of each histological variation; a previous study correlating quantitative histology with ex-vivo relaxometry in human lung tumours has clearly illustrated the difficulty in discussing NMR parameters with respect to histology [27].

Furthermore, the speed of exchange between bound and free water determines if there is a mean relaxation time or two or more separately detectable relaxation times: in healthy muscle, it has been established that two spin-spin relaxation times can be separately identified expressing a slow exchange between different water phases [28,29].

Table 2 T1 and T2 frequency dependence of human skeletal muscle in-vivo measured on 13 MRI units after correction resulting from a preliminary quality assessment using Eurospin TO5 test object [26]

NMR frequency	4.3 MHz	11.9 MHz	21 MHz	63 MHz
Number of in-vivo measurements	70	12	330	162
Mean T1 (ms)	223 +/− 31	557 +/− 26	557 +/− 41	1183 +/− 136
Mean T2 (ms)	34 +/− 3	42 +/− 2	34 +/− 4	33 +/− 5

All these considerations clearly demonstrate that the interpretation of voxel grey level is highly complex and must be prudently related to histological changes. The challenge is therefore to develop a pulse sequence potentially able to differentiate histological changes [30].

What texture parameters are mainly used in MR images analysis?

The first-order features are based only on the distribution of pixel grey levels and do not consider the relationships between neighboring pixels. They could contain some useful information in terms of tissue differentiation. They provide knowledge on the most frequent and the least frequently occurring grey levels, on the concentration of the grey levels around their average, or on the degree of asymmetry in their distribution.

When a MR image is suspected to contain a plurality of strips or beam-like structures, a method for its texture characterization seems to be the run-length matrix-based approach [31] (Figure 1 left). In such a method, the parameters are determined by the presence, the length, and the orientation of pixel runs (strings), composed of pixels with quite similar grey levels. With a certain adjustment of the method, it is possible to obtain the parameters that enhance (or not) a particular orientation of pixel runs (horizontal, vertical, or oblique, with $\theta = 45°$ or $\theta = 135°$). It is also possible to decide which differences in pixel grey levels within a single run are to be ignored. The run-length matrix-based features could emphasize the incidence of relatively short (or relatively long) runs, measure the non-uniformity of grey levels (or run lengths), or give the information about the fraction of image in runs.

Very important information could also be extracted with the co-occurrence matrix-based method [32] (Figure 1, right). This method analyses the co-occurrences of pairs of pixels, spaced apart a specified distance, d, and aligned with a given direction, θ. All the possible signed differences in grey levels of pixels are considered. A similar method, based on grey-level difference matrices [33], considers only the unsigned differences. With a properly chosen distance for pixel pairs (the parameter d of both methods) one

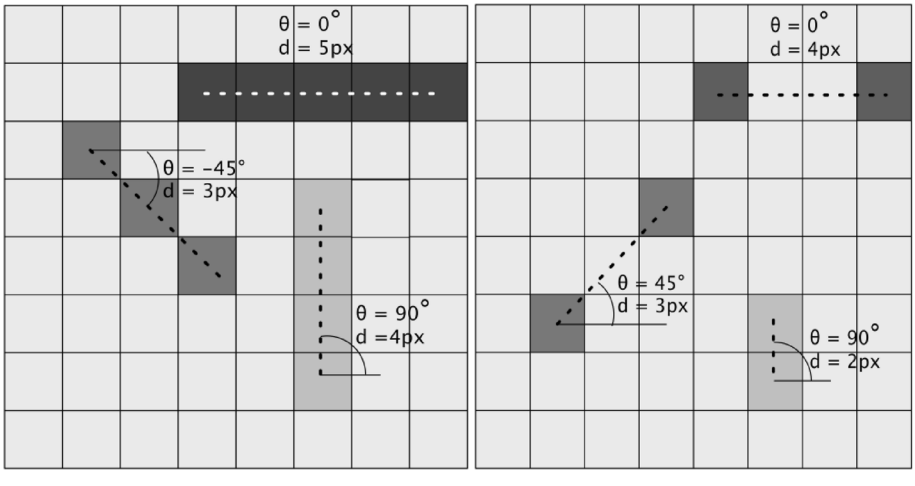

Figure 1 Illustration of the pixel relationship considered by the Run-length matrix approach (left) and the Cooccurrence matrix method (right).

can obtain the features sensitive to the presence or absence of different image elements (primitives). If certain texture structures appear in the image, or change their size, with the disease development, the features based on the pixel grey level difference matrices will also change (if the distance parameter, d, is constant). If two textures are characterized by different co-occurrence matrix-based parameters, it could be highly probable, that they correspond to different stages of the disease. As the parameter d depends on the image scale and the size of texture primitives, it is worthwhile to fix it experimentally.

Several texture parameters can be derived from the co-occurrence matrix with a given pair of parameters: (d,θ). Among them it is worth mentioning: energy or angular second moment (a measure of homogeneity of pixel grey levels, relatively high for homogeneous textures, and of small values for heterogeneous ones), contrast or inertia (with a quite large value for heterogeneous regions, characterized by a strong contrast, and quite small value for homogeneous regions), local homogeneity, and entropy (that quantifies the degree of randomness of pixel grey levels).

The ripples can also be extracted with a method based on image transformations using the Laws' filters. During the transformation, each image pixel is assigned a value that is a linear combination of initial grey levels of pixels belonging to the neighborhood of a transformed pixel. Typically neighborhoods of 3×3 or 5×5 pixels are considered. Weights of grey levels of neighboring pixels are determined by one of the Laws' masks. The masks are designed in order to detect different texture elements: ripples, edges, spots… The frequency rate of such elements determines the feature values calculated from the transformed image.

Another group of features, that could be used to indicate the presence of edges are those derived from the gradient matrices [34]. The grey-level gradient at a given image point depends on the differences between the grey levels of its neighboring pixels, located on lines (vertical and horizontal) intersecting at a point. The gradient matrix contains the values of the absolute gradient at each point of the image region considered. Based on the gradient matrix several first order statistics can be calculated. Apart of being edge-sensitive, such statistics allow us to draw conclusions about the uniformity (homogeneity) or the roughness of the texture. These latter texture properties are closely related to changes in the muscular tissue that occur during the development of the disease.

Moments, either continuous or discrete, rely on a very rich theory and encompass a wide family (Legendre, Zernike, Tchebichef, Racah, etc. [35]). They have been used in a large variety of problems including segmentation, pattern recognition, image reconstruction, watermarking. Although not often applied to texture analysis, they offer several interesting and unique properties among which their applicability to high dimensional space, their capability to capture low and high frequency components according to the selected order and the possibility to deal with noise and blurring. They not only allow the analysis of images but also allow the reconstruction of them using the computed moment values and thus permit the identification of the information they captured. Moment invariants to geometric transform (translation, rotation, scale) can be derived too [36,37] with a good stability to non-rigid and small local deformations.

Combining texture descriptors is a way to improve their discriminative power and can offer a tool to characterize a lesion.

Previous results in muscle MRI-TA

Sikio et al. [20] used co-occurrence matrix parameters on T2 weighted images such as the angular second moment, the inverse difference moment, the entropy and the difference entropy to describe the muscle tissue structure and the effect of different types of exercise. By mean of the Mann–Whitney statistical test, the study revealed exercise-load-associated differences in MRI textures of thigh soft tissues between various athlete groups and non-athletes. For each muscle of the thigh, each texture parameter was considered individually and the non-athletes group was compared to each of the five groups of athletes. The result showed that large variation in tests significance were observed depending on the muscle, the texture parameter used and the comparison performed. The authors did not show how the texture parameters evolve for athletes when compared to the non-athletes one, however they related the changes in texture descriptors to the change of the muscle architecture according to the type of exercise as well as the type of the muscle.

In the same way, Nketiah et al. [38] have detected texture differences in MRI of hip muscles associated with different level of long term exercise loading in female athletes (jumpers) and controls.

In pathological cases, texture analysis of MRI data can be a valuable tool to monitor the changes that occur to the muscle tissue. For instance, Skoch et al. [21] were interested in the classification of calf muscle of patients with different pathology. They scanned 93 volunteers (20 healthy and 73 with three types of pathology) and extracted texture parameters from T1 weighted images using MaZda software [39]. For dimensionality reduction, the author used Principal Component Analysis (PCA) to extract a group of features that best characterized each muscle. The projection on the two first principal components showed that no difference existed between control groups and healthy ones with hypertonic parents. In opposition, the healthy group and the patients with diabetes mellitus group could be linearly separated. Considering that different pathology had different impact on the muscle appearance, four groups scored by radiologists were created: 1) muscles without any visible signs of pathology, 2) muscles with mild pathological or nonspecific changes, 3) muscles with marked pathological or nonspecific changes such as apparent muscle atrophy or fat infiltration, 4) muscles with severe pathological changes or muscles almost complete replacement by fat. The projection of the different muscle on the two main axis of the PCA showed that the 4^{th} muscle group is well separated from the others and PCA should be performed in subgroups 1, 2 and 3 to obtain better discrimination between muscles with moderate infiltration. The results obtained in the paper suggested that TA can be used as an objective tool for MR images evaluation and the results correlated well with the clinical status of patients.

Following almost the same scheme, a study carried out by Herlidou et al. [2] compared TA techniques to the assessment of several radiologists, on a set of data obtained from patients with muscular dystrophy and healthy volunteers. The texture descriptors such as histogram, co-occurrence matrix, gradient matrix and run length matrix, were extracted from T1 weighted images. In parallel, the radiologists were asked to characterize each ROI by rating the contrast, the texture coarseness, the texture complexity, the strength and the fat infiltration. The analysis of the texture parameters was achieved using Correspondence Factorial Analysis (CFA) resulting in an healthy and patient volunteer automatical classification with sensitivity of 70% and specificity of 86%. Visual inspection

by radiologists that were blinded to clinical information provided less accurate classification (sensitivity of 56% and specificity of 71%). In addition to that, very significant differences were observed between the radiologist's assessments of texture features. Besides a large intra-observer variability was noted. All these studies confirm that TA can offer an objective and reliable tool for tissue characterization though the interpretation of the data still remains speculative. This is why the MYO-MRI European COST action recently has started a multicentre study based on a data set of MR images of Golden Retriever Muscular Dystrophy (GRMD) dogs.

Histological changes during the GRMD course

Duchenne Muscular Dystrophy (DMD) is a human muscular disease caused by mutations in dystrophin genes and characterized by a progressive muscle atrophy and weakness. GRMD dog is the commonly used animal model of human DMD with similar clinical and pathological disease evolution [40]. Necrosis, inflammation, fat infiltration and fibrosis progressively occur. The histological expression of the disease follows the clinical evolution up to death [41] (Figure 2).

From birth to 3 months of age, GRMD skeletal muscles displayed hypercontracted and degenerating isolated fibers [42]. Up to 3 months, these fibers are rather low in number, specially in extensor muscles, and are associated with many large clusters of regenerating fibers. After this first regenerative period, another period begins from about 3 to 6 months of age and is marked by a dramatic increase in the number of degenerating necrotic fibers, sometimes appearing in clusters [43,44]. This degenerative phase is associated with a low regenerative activity [45]. At this stage, skeletal muscle tissue displays early evidences of endomysial oedema and mild fibrosis with some minimal to mild infiltration by inflammatory cells. The last period begins from 6 months of age, and is a rather slow evolution period. Degeneration and regeneration still occurs at a lower level and intensity of fibrosis and fat tissue infiltration progressively increases [46] although some authors do not confirm this result. Scattered calcification foci may be present but their frequency strongly differs between GRMD dogs. When present, these mineral deposits elicit a strong local inflammatory response (Table 3). Clinically a dramatic decrease of muscular functions is observed from about 2 to 6 months of age corresponding to the tissue degenerative period and precedes a period of paradoxical stability during the next months until some major digestive or respiratory complications occurs.

How histological changes during GRMD disease modify NMR parameters?

As the histological variations (inflammation, fibrosis, necrosis, fat infiltration…) do not modify relaxation times in the same way, in the same proportion and at the same time, the final result (i.e. the pixel grey level) is rather difficult to be strictly interpreted in terms of histology, especially when two simultaneous tissue changes modify a relaxation time in opposite directions.

During GRMD disease evolution, T1 is first increased due to an increase of muscle free water concentration related to muscle degeneration-regeneration and inflammation. Later T1 decreases in relation to fibrosis and fat infiltration. T2 is longer in necrotic but also in fatty and connective tissue. Therefore the distinction between necrosis, fat infiltration or fibrosis cannot be easily performed. As the dystrophic process results

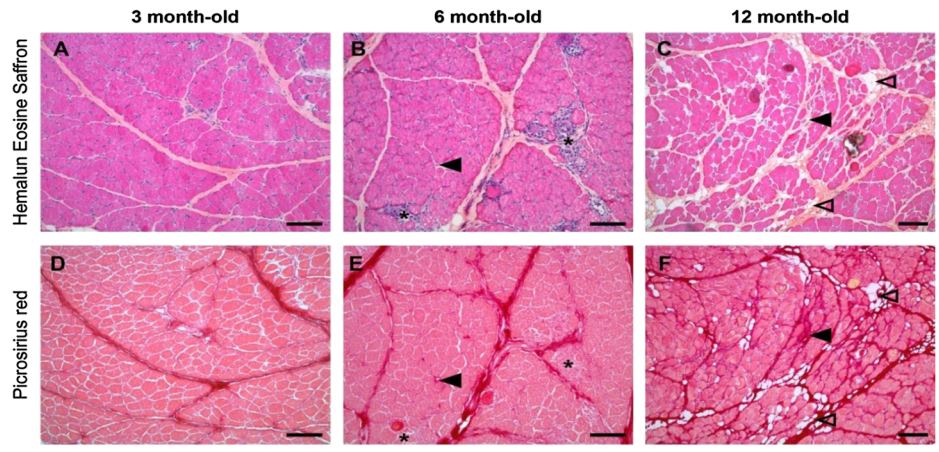

Figure 2 Typical histopathological presentation of skeletal muscles of GRMD dogs, 3, 6 and 12 month-old. Changes are mild at 3 months **(A)** with only some hypercontracted hyaline fibers, and a diffuse increase in cell number mainly due to a regenerative activity. At 6 months, degenerative and necrotic changes are more severe, focally associated with some inflammatory cell infiltration (*). At 12 months, fibrotic (black arrowhead) and fat tissues (open arrowhead) are proeminent. **(A-C)** Hemalun eosin saffron and (E-F) Picrosirius red stainings for fibrotic tissue. Bars = 100 μm **(A-B, D-E)** and 200 μm **(C and F)**.

in a muscle tissue disorganization, heterogeneous signal distribution within diseased muscle is expected, leading to the potential interest in MRI TA. This has been better observed in T2 weighted images.

Then, if the image grey level is rather difficult to analyze in terms of histology, it can be expected that the tissue texture can be more informative with MRI-TA. MRI texture results from the contrast between different parts of the tissue (for instance fibrosis, fat infiltration, inflammation, etc.), this contrast itself resulting from the effect of histological parameters on NMR parameters.

To illustrate the scale gap between histology and MRI, Figure 3 represent the same three histological images (Hemalun eosin saffron staining) at an MRI scale by addition of pixels fsrom the histological images.

MRI-TA results on GRMD dogs

The simplest texture parameter was the standard deviation or the heterogeneity parameter introduced by Thibaud et al. [22] in T2 weighted images. The authors compared the tissue heterogeneity between healthy and GRMD dogs at different age group (from 2

Table 3 Histological evolution during GRMD disease

Period	Regenerative	Degenerative	Slowly evolutive
Age (months)	2-3	5-6	9-12
Hyalin fibers	mild	marked to severe	marked
Necrosis	mild	marked to severe	marked
Regeneration	marked	mild	minimal
Centronucleated fibers	minimal	mild	marked
Inflammation	none	inconstant	mild
Fibrosis	none	mild to marked	marked to severe
Adiposis	none	minimal	mild

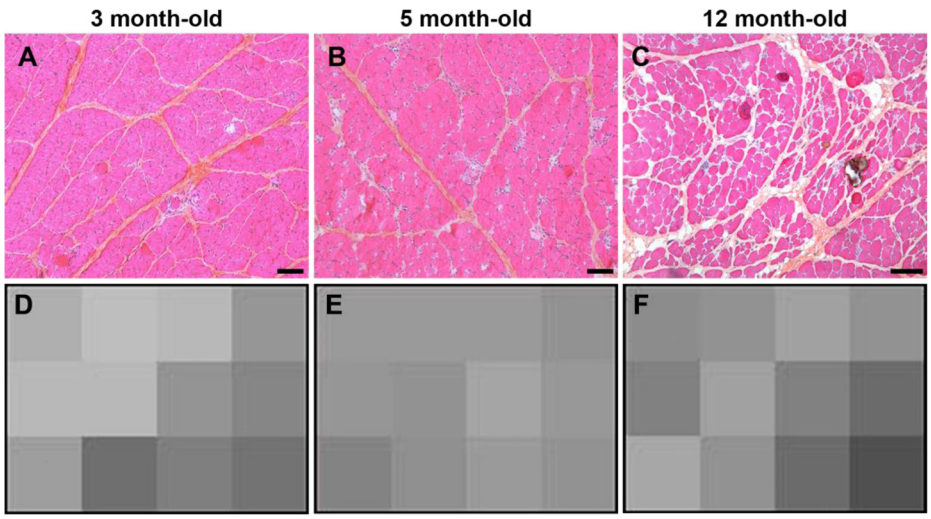

Figure 3 Typical histopathological presentation of skeletal muscles of GRMD dogs, 3, 5 and 12 month-old and corresponding images at an MRI scale. Progressive tissue changes characteristic of the disease evolution elicited some heterogeneity in the tissue aspect. This heterogeneity increases with age as the disease progress and the muscle tissue is replaced by fibrosis and some adipose tissue infiltration. **(A-C)** Hemalun eosin saffron and **(D-F)** Mean grey level of the histological images **A**, **B** and **C** were transformed to images **D**, **E** and **F** at an MRI resolution. Mean value was sampled using region of interest of 320 pixels **(A-B)** or 648 pixels **(C)** and consecutively converted to greyscale. Bars = 100 μm **(A-B)** and 200 μm **(C)**. Pixel size = 0.91 μm **(A-B)** and 0.78 μm **(C)** for histological images, 290 μm **(D-E)** and 500 μm **(F)** for MRI-simulated corresponding images.

months to 9 months). Comparison of groups was made using statistical tests to check if there were significant differences between them. The results showed that GRMD heterogeneity indices were significantly higher than in healthy dogs by at least 40% at all ages.

First order texture parameters such as mean grey levels, kurtosis or skewness clearly differ in histological Figure 3A, B and C and then are suspected to also differ in MRI-TA during the three steps of the GRMD disease as illustrated by the simulated MR images 3D, 3E and 3F.

Fan et al. [47] studied GRMD at 6 months of disease evolution: first order texture descriptor like entropy as well as higher order descriptors like the run length matrix were calculated using T2 weighted images to characterize the muscle tissue. The Mann–Whitney-Wilcoxon test showed that for all ages (3, 6 and 9–12 months), all texture features were significantly higher in GRMD when compared to healthy dogs. In addition to that, a linear discriminant analysis was performed where each NMR biomarker, including texture parameters, were used in addition with age as input variables and the group (GRMD or normal) as a response. The results showed that texture parameters extracted from the run length matrix had in average a better discriminant power than other NMR biomarkers such as the fat content and the relaxation time T2 that can be seen as an indicator of an inflammatory process. The best discriminant parameters were the ones related to muscle morphology. The entropy was not a good discriminant between healthy and GRMD dogs. For some muscles, a correlation between NMR biomarkers and histopathology indices (fibrosis, fiber number, fiber size etc.) was performed but texture parameters did not show a significant correlation with them; this lack of correlation has been explained by the scale difference because texture analysis

was done at the macro level (minimal unit of voxel is $1 \times 1 \times 1$ mm^3), while histopathological data are represented at micro level (a scale of around 50 μm for fiber diameter).

In spite of the encouraging results obtained with a first order parameter, it is very important to consider other texture descriptors that provide information about the spatial organization of the tissue. Preliminary results on GRMD dogs from MYO-MRI COST action have already established that some texture methods discriminate early disease stages while others are more interesting for later phases of disease evolution. The MRI-TA study from Duda et al. [Differentiation based on MRI texture analysis between GRMD and healthy dogs at different phases of the disease evolution, in preparation] on GRMD dogs using textural features derived from different approaches (statistical, filtering-, and model-based) have demonstrated an early detection at 2–3 months with a percentage of correctly recognized cases reaching even nearly 99%. In this study, 8 methods for texture analysis were tested, including: grey-level histograms, autocorrelation coefficients, gradients, co-occurrence matrices, run length matrices, grey level difference matrices, factional Brownian motion model, and Laws' texture energy measures. In addition, a feature selection was performed, in order to assess the relative importance of each feature, in terms of the classification accuracies. The results differed between different types of muscles. Nevertheless, the application of some groups of features very often led to obtain satisfactory results. Among the top methods were: the co-occurrence matrix-based, grey-level differences matrix-based, gradient-based, histogram-based, Laws' filtering, and run-length matrix-based. The features from the co-occurrence matrices were top ranked for the early stage of GRMD development, while the run length-based method ensured the best tissue recognition for the final stage of canine life.

Conversely, another MRI-TA study of GRMD dogs from Yang et al. [Differentiation based on MRI texture analysis between GRMD and healthy dogs at different phases of the disease evolution, submitted], using orthogonal moments has not differentiated the early stage (2–3 months) but appeared efficient for disease follow-up during later stages.

Snezhko et al. [48], on the same set of GRMD image data, have extracted 313 texture features from MaZda software: a combination of several selected texture features have, for instance, have allowed an early (month 2) detection of the disease with an accuracy of 97% using cross-validation with leave-one-out strategy. For larger muscles, the efficiency of all the features was better than for smaller muscles. It was likely due to the size (number of voxels) of the available ROI.

The preliminary choice of TA methods and features should be done taking into account not only the particular development of GRMD-related pathological changes (detected on histological or MR images), but also other, not texture-related constraints. As regards the regions of interest, defined on GRMD muscles, they could be very small, in particular for the first stage of canine life. Moreover, they are usually thin and narrow. This excludes the use of many methods and parameters that have proven to be reliable in other texture-based classification tasks. For example, the run-length matrix-based method could be less useful for the small, tiny ROIs that have only few pixels of length or width. The larger is the ROI, the more useful will be the parameters based on pixel runs. This could explain why the run-length matrix-based features turned out to be reliable for tissue differentiation at the final stage of canine life. The same comments also apply to the co-occurrence matrix-based or grey level difference matrix-based methods

with a parameter d of a large value. Here, a good solution would be to set a d parameter to 1 or, maximum, to 2 pixels. Finally, the first-order features, derived from the grey-level histograms, could be calculated for ROIs of any size.

As the ROI size could differ from one case to another, especially when it is determined by the age of the canine, an important task is the choice of features independent of ROI size. Admittedly, it can be predicted, that features obtained for a relatively large d will not be suitable to characterize small ROIs. It could even be problematic to calculate them. However, among the features considered potentially useful, some may be too unstable (dependent on the ROI size and/or position) to consider them as reliable texture descriptors [49]. Experimental analysis of the features stability, performed on MR images or phantoms, should therefore precede the classification experiments, in order to exclude *a priori* the features that could not really contribute to a muscular tissue recognition.

Conclusion

The MRI contrasts, depending on the incidence of histological components on relaxation parameters and spin density, determines the MRI texture. Then, two key problems have still to be more deeply discussed: i) How histological components modify MRI contrasts and then texture? and ii) How texture at the MRI scale can be related to histological texture at a very different scale? These two questions corresponds to the shared goals of our multicentre research group under the auspices of the European Union COST MYO-MRI action and is undoubtedly a prerequisite for a larger diffusion of clinical MRI-TA.

The way to bridge the scale gap should be based on the correlation of MRI-TA and the histological changes seen on the biopsies. However, a direct correlation between MRI and biopsy at the histological scale is probably not a reachable challenge. This complex comparison only would be possible under two premises. First, it will be necessary to use exactly the same samples for both analyses, requiring a stereotactic biopsy. Secondly, the histological analysis should be precise, objective and quantitative. Recently, a new computer based image analysis method has been developed to improve the evaluation of muscle biopsies [50,51]. This approach not only extracts important geometric parameters such as the size of the slow and fast fibers or the content of collagen, but also captures the organization of the tissue. The images are converted in a graph of fiber to fiber contacts. In this way it is possible to obtain certain global features that are relevant to objectively evaluate human muscular dystrophies. The quantification of the changes of these selected features will be a key to compare these images with their corresponding MRI-TA.

Competing interests
The authors declare that they have no competing interests.

Authors' contributions
JDC carried out introduction, conclusion and participated to "The scale gap between histology and MRI" and "What MRI factors dictate the pixel grey level" and drafted a large part of the manuscript. TL carried out "Histological changes during the GRMD course". TL and JDC carried out "How histological changes during GRMD disease modify NMR parameters". DD, NA, JLC and PAE carried out "What texture parameters are mainly used in MR images analysis". RAL carried out "Previous results in muscle MRI-TA". AMGP and MP carried out "Perception of visual texture". DD, LME, GY, ES and AS carried out "MRI-TA results on GRMD dogs". All authors read and approved the final manuscript.

Author details
[1]Institute of Myology, NMR laboratory, Paris, France. [2]CEA, I2BM, MIRCen, NMR laboratory, Paris, France. [3]INRA, UMR 703 PAnTher, Oniris, Nantes, France. [4]Faculty of Computer Science, Bialystok University of Technology, Bialystok, Poland. [5]PRISM-BioSCANs, University of Rennes, Rennes, France. [6]Instituto de Biomedicina, CSCIC Universidad de Sevilla, Sevilla, Spain. [7]University da Beira Interior, Covilha, Portugal. [8]LIST, Southeast University, Nanjing, China. [9]LTSI, INSERM, University of Rennes, Rennes, France. [10]Lab. Of Mathematical Cybernetics, UIIP, Belorussian Academy of Science, Minsk, Belarus. [11]Ninewells Hosp. and Medical School, Dundee, Scotland, United Kingdom.

Received: 12 December 2014 Accepted: 18 February 2015
Published online: 19 March 2015

References

1. For review, Hajek M, Dezortova M, Materka A, Lerski RA. Texture Analysis for Magnetic Resonance Imaging. Prague: Med4Publishing; 2006.
2. Herlidou S, Rolland Y, Bansard JY, Le Rumeur E, de Certaines JD. Comparison of automated and visual texture analysis in MRI: characterization of normal and diseased muscle. Magn Reson Imaging. 1999;17(9):1393–7.
3. Mahmoud-Ghoneim D, Cherel Y, Lesoeur J, Lemaire L, Rocher C, de Certaines JD, et al. Texture analysis of MR Images of rat muscles during atrophy and regeneration. Magn Reson Imaging. 2006;24(2):167–71.
4. Mamhoud-Ghoneim D, Bonny JM, Renou JP, de Certaines JD. Ex-vivo Magnetic Resonance Imaging Texture Analysis can identify genotypic origin in bovine meat. J Sci Food Agric. 2005;85:629–32.
5. Nguyen F, Eliat PA, Pinot M, Franconi F, Lemaire L, de Certaines JD, et al. Correlations between Magnetic Resonance Imaging and histopathology in mdx (X-linked Muscular Dystrophy) murine model of Duchenne Muscular Dystrophy, 24th congress of the European Society of Veterinary Pathology, Edinburgh. 2006.
6. Rosenholtz R. Texture perception. In: Wagemans J, editor. Oxford Handbook of Perceptual Organization (in press). Oxford, U.K: Oxford University Press; 2014.
7. Landy MS. Texture Perception. In: Adelman G, editor. Encyclopedia of Neuroscience. Amsterdam: Elsevier; 1996.
8. Giora E, Casco C. Region- and edge-based configurational effects in texture segmentation. Vis Res. 2007;47(7):879–86.
9. Machilsen B, Wagemans J. Integration of contour and surface information in shape detection. Vis Res. 2011;51:179–86.
10. Julesz B. Visual Pattern Discrimination. IRE Transactions on Information Theory. 1962;8(2):84–92.
11. Julesz B. Texture and Visual Perception. *Scientific American*, 212, 38–48. Julesz, B. (1975). Experiments in the visual perception of texture. Sci Am. 1965;232(4):34–43.
12. Julesz B, Gilbert EN, Victor JD. Visual discrimination of textures with identical third- order statistics. Biol Cybernet. 1978;31:137–40.
13. Klein SA, Tyler CW. Phase discrimination of compound gratings: generalized autocorrelation analysis. J Opt Soc Am A. 1986;3:868–79.
14. Malik J, Perona J. Preattentive texture discrimination with early vision mechanisms. J Opt Soc Am A. 1990;7:923–32.
15. Tyler CW. Theory of texture discrimination based on higher-order perturbations in individual texture samples. Vis Res. 2004;44:2179–86.
16. Heeger DJ, Bergen JR. Pyramid-based texture analysis/synthesis. In: Proceedings of the 22nd annual conference on Computer graphics and interactive techniques (SIGGRAPH'95). Los Angeles (USA): IEEE Comput. Soc. Press; 1995. p. 229–38.
17. Portilla J, Simoncelli EP. A Parametric Texture Model Based on Joint Statistics of Complex Wavelet Coefficients. Int J Comput Vis. 2000;40(1):49–71.
18. Rosenholtz R. Significantly different textures: A computational model of pre-attentive texture segmentation. In D. Vernon (Ed.), Proc. European Conf. on Computer Vision (ECCV'00). LNCS. 2000;1843:197–211.
19. Nothdurft HC. Texture segmentation and pop-out from orientation contrast. Vis Res. 1991;31(6):1073–8.
20. Sikio M, Harrison LCV, Nikander R, Ryymin P, Dastidar P, Eskola HI, et al. Influence of exercise loading on MRI texture of thigh soft tissue. Clin Physiol Funct Imaging. 2014;34:370–6.
21. Skoch A, Jirak D, Vyhnanovska P, Dezortova M, Fendrych P, Rolencova E, et al. Classification of calf muscle MR Images by texture analysis. Magma. 2004;16:259–67.
22. Thibaud JL, Monnet A, Bertoldi D, Barthélémy I, Blot S, Carlier PG. Characterization of dystrophic muscle in Golden Retriever Muscular Dystrophy dogs by nuclear magnetic resonance imaging. Neuromuscul Disord. 2007;17(7):575–84.
23. Wang J, Fan Z, Vandenborne K, Walter G, Shilhoh-Malmawsky Y, An H, et al. A computerized MRI biomarker quantification scheme for a canine model of Duchenne muscular dystrophy. Int J CARS. 2013;8:763–74.
24. Bottomley PA, Foster TH. Argensinger R.E?, Pfeiffer L.M., A review of normal tissue hydrogen NMR relaxation times and relaxation mechanisms from 1–100 MHz: Dependence on tissue type, NMR frequency, temperature, species, excision and age. Med Phys. 1984;11(4):425–48.
25. Henriksen O, de Certaines JD, Spisni A, Cortsen M, Muller RN, Ring PB. In-vivo field dependence of proton relaxation times in human brain, liver and skeletal muscle: a multicenter study: ii. Magn Reson Imaging. 1993;11:851–6.
26. de Certaines JD, Henriksen O, Spisni A, Cortsen M, Ring PB. In-vivo measurement of proton relaxation times in human brain, liver and skeletal muscle: a multicenter study: i. Magn Reson Imaging. 1993;11:841–50.
27. Bernard AM, De Certaines JD, Delaval P, Louvet M, Coetmeur D. Histological explanation of proton T1 and T2 variations in human lung tumors. In: Allen PS, Boisvert DPJ, Lentle BC, editors. Magnetic resonance in cancer. Toronto (Canada): Pergamon press; 1986. p. 49–50.
28. Le Rumeur E, de Certaines J, Toulouse P, Rochcongar P. Water phases in rat striated muscles as determined by T2 proton NMR relaxation times. Magn Reson Imaging. 1987;5(4):267–72.
29. Araujo ECA, Fromes Y, Carlier PG. New insights on human skeletal muscle tissue compartments revealed by in-vivo T2 NMR relaxometry. Biophys J. 2014;106:2267–74.
30. Lerski RA, de Certaines JD, Duda D, Klonowski W, Yang G, Coatrieux JL, et al. Application of texture analysis to muscle MRI: 2- Technical recommendations. EPJ Nonlinear Biomedical Physics 2015, 3:2.

31. Galloway MM. Texture analysis using grey level run lengths. Computer Graphics and Image Processing. 1975;4:172–9.
32. Haralick RM, Shanmugam K, Dinstein I. Textural features for image classification, IEEE Transactions on Systems. Man Cybernetics. 1973;3:610–21.
33. Weszka JS, Dyer CR, Rosenfeld A. A Comparative Study of Texture Measures for Terrain Classification, IEEE Trans. Systems, Man, Cybernetics. 1976;6:269–85.
34. Lerski RA, Straughan K, Shad L, Boyce D, Bluml S, Zuna I. MR Image Texture Analysis - An Approach to Tissue Characterization. Magn Reson Imaging. 1993;11:873–87.
35. Shu H, Luo L, Coatrieux J-L. Moment-based approaches in imaging. Part 1, basic features. IEEE EngMedBiol Magazine. 2007;5:70–4.
36. Shu H, Luo L, Coatrieux J-L. Derivation of moments invariants. In: Papakostas GA, editor. Moments and moments invariants. Xanthi (Greece): Science Gate Publishing; 2014.
37. Chen B, Shu H, Zhang H, Coatrieux G, Luo L, Coatrieux J-L. Combined invariants to similarity transformation and to blur using orthogonal Zernike moments. IEEE Trans Image Process. 2011;20(2):345–60.
38. Nketiah G, Savio S, Dastidar P, Nikander R, Eskola H, Sieväwen H. Detection of exercise load-associated differences in hip muscles by texture analysis. Scand J Med Sports. 2014;20:10.1111.
39. Szczypinski P, Strzelecki M, Materka A, Klepaczko A. MaZda-A software package for image texture analysis. Comput Methods Prog Biomed. 2009;94(1):66–76.
40. Kornegay JN, Bogan JR, Bogan DJ, Childers MK, Li J, Nghiem P, et al. Canine models of Duchenne muscular dystrophy and their use in therapeutic strategies. Mamm Genome. 2012;23(1–2):85–108.
41. Kornegay JN, Tuler SM, Miller DM, Levesque DC. Muscular dystyrophy in a litter of golden retriever dog. Muscle Nerve. 1988;11:1056–64.
42. Nguyen F. Muscle Lesions Associated with Dystrophin Deficiency in Neonatal Golden Retriever Puppies. J Comp Pathol. 2002;126(2–3):100–8.
43. Valentine BA, Cooper BJ, Cummings JF, de Lahunta A. Canine X-linked muscular dystrophy: morphologic lesions. J Neurol Sci. 1990;7(1):1–23.
44. Cooper BJ, Winand NJ, Stedman H, Valentine BA, Hoffman EP, Kunkel LM, et al. The homologue of the Duchenne locus is defective in X-linked muscular dystrophy of dogs. Nature. 1988;334(6178):154–6.
45. Cozzi F, Cerletti M, Luvoni GC, Lombardo R, Brambilla PG, Faverzani S, et al. Development of muscle pathology in canine X-linked muscular dystrophy. II. Quantitative characterization of histopathological progression during postnatal skeletal muscle development. Acta Neuropathol. 2001;101(5):469–78.
46. Nguyen F, Guigand L, Goubault-Leroux I, Wyers M, Cherel Y. Microvessel density in muscles of dogs with golden retriever muscular dystrophy. Neuromuscul Disord. 2005;15(2):154–63.
47. Fan Z, Wang J, Ahn M. Characteristics of magnetic resonance imaging biomarkers in a natural history study of golden retriever muscular dystrophy. Neuromuscul Disord. 2014;24:178–91.
48. Snezhko EV, Carlier P, Kovalev VA, Azzabou N, Dmitruk AA, Shukelovich AV. Application of Texture Analysis Techniques on NMR Images for Quantitative Assessment of Muscle Disorders. Informatics. 2014;3:5–13.
49. Duda D. Medical image classification based on texture analysis. PhD Thesis, University of Rennes 1, Rennes, France, 2009.
50. Sáez A, Acha B, Montero-Sánchez A, Rivas E, Escudero LM, Serrano C. A., Neuromuscular disease classification system. J Biomed Opt. 2013;18(6):66017.
51. Sáez A, Rivas E, Montero-Sánchez A, Paradas C, Acha B, Pascual A, et al. Quantifiable diagnosis of muscular dystrophies and neurogenic atrophies through network analysis. BMC Medicine. 2013;11:77.